Heteroaryl-Substituted Bis-Anils: Aggregation-Induced Emission (AIE) Derivatives with Tunable ESIPT Emission Color and pH Sensitivity

Timothée Stoerkler, Pascal Retailleau, Gilles Ulrich, Denis Jacquemin, Julien Massue

Heteroaryl-Substituted bis-Anils: Aggregation-Induced Emission (AIE) Derivatives with Tunable ESIPT Emission Color and pH Sensitivity

Timothée Stoerkler,[a] Dr. Pascal Retailleau,[b] Prof. Dr. Denis Jacquemin,[c],[d] Dr. Gilles Ulrich[a] and Dr.Julien Massue[a]*

[a] Institut de Chimie et Procédés pour l'Energie, l'Environnement et la Santé (ICPEES), Equipe Chimie Organique pour la Biologie, les Matériaux et l'Optique (COMBO), UMR CNRS 7515, Ecole Européenne de Chimie, Polymères et Matériaux (ECPM), 25 Rue Becquerel, 67087 Strasbourg Cedex 02, France

[b] Service de Cristallographie Structurale, ICSN-CNRS, Université Paris-Saclay 1 Avenue de la Terrasse, Bât. 27, 91198 Gif-sur-Yvette Cedex, France

[c] Nantes Université, CNRS, CEISAM UMR 6230, F-44000 Nantes, France

[d] Institut Universitaire de France (IUF), F-75005, Paris, France

Email: massue@unistra.fr

https://twitter.com/JulienMassue

Abstract

The two-step synthesis, structural, and photophysical properties of a series of heteroaryl-substituted bis-anil derivatives presenting aggregation-induced emission (AIE) coupled with an excited-state intramolecular proton transfer (ESIPT) process is described. The fluorescence color of the aggregates can be fine tuned by changing the electronic nature of the peripheral substitution, leading to a wide range of emission wavelengths (from green to the near infra-red). Moreover, upon introduction of strong electron-withdrawing groups such as cyano (CN), a competition between ESIPT and deprotonation is observed leading to the emission of the anionic species at low water percentage. This observation led to the synthesis of an additional mixed AIE fluorophore, functionalized by methoxy groups on one side and cyano groups on the other side. Upon addition of water, this dye displays first anionic emission, followed by typical AIE/ESIPT red fluorescence upon formation of the aggregates. TD-DFT calculations on selected AIE dyes were performed to rationalize the nature of the emissive transitions in these derivatives.

Introduction

Aggregation-induced emission (AIE) is a photophysical process typically observed in rotor-shaped molecular scaffolds showing faint to no emission in dilute solution, due to important vibrational and rotational relaxations. In contrast, strong luminescence enhancement is achieved in concentrated media such as aggregates or nanoparticles, owing to a restriction of intramolecular motions (RIM).[1] This phenomenon, developed and popularized by Tang, has been evidenced in hydrocarbon scaffolds such as tetraphenylethylene (TPE),[2] as well as in a wide range of others structures containing heterocycles[3] and/or supramolecular assemblies.[4] A significant improvement was the combination of Excited-State Intramolecular Proton Transfer (ESIPT) process and AIE fluorescence. ESIPT is a four-level photocycle process occurring in five- or six-membered H-bonded fluorophores, leading to red-shifted and environment-sensitive emission.[5] The ESIPT process can efficiently amplify the AIE effect through its strong molecular reorganization in the excited-state and inherent H-bonded network. Moreover, the large Stokes' shifts associated with ESIPT dyes help avoiding inner-filter effect and self-quenching at high concentrations, while the absence of π-stacking combined with RIM enhances the overall radiative process in aggregated media. AIE-coupled ESIPT fluorescence has been evidenced in various solid matrixes, including aggregates, showing red-shifted fluorescence emission, with a strong charge transfer (CT) character.[6] Over the years, a growing number of AIE/ESIPT derivatives has been reported, based on various structures including 2-(2'-hydroxyphenyl)-benzazole or triphenylamine-salicylaldehyde,[7] and others[8] These dyes have found applications as light-harvesting systems in electroluminescent devices,[9] stimuli-responsive materials in security inks and switches,[10] as well as for the detection of multiple analytes[11] or the monitoring of intracellular processes.[12] Ratiometric determination of pH, a key parameter in biological processes, is a fundamental challenge in microenvironments or organelles such as lysosomes, as a misregulation of intracellular pH is associated with numerous diseases.[13] Examples of pH-sensitive multicolor ESIPT probes, capable of fine-tuning their fluorescence color or modify their optical profiles, either via *on-off* or *off-on* processes[14] or by ratiometric modulation of the intensity between two emission bands,[15] as a function of pH can be found in the literature. Nevertheless, it appears therefore important to develop additional families of pH-sensitive AIEgens showing ESIPT with efficient and expedite syntheses, improved AIE behaviour, enhanced (photo)stability and possibility to fine-tune the fluorescence color. Chemical engineering studies around AIE molecular cores, *i.e.*, systematic investigation of the modulation of the AIE fluorescence color by structural modification have proved necessary in order to build ground rules for the design of smart AIE-ESIPT units.[16] A well-reported strategy to develop AIE/ESIPT derivatives is to covalently associate TPE units with ESIPT moieties, such as imino-phenol (anil) moieties.[17] Other studies include AIE-active anil derivatives, without the association of TPE units for drug delivery applications or the use of dimers (bis-anils) as AIEgen but precipitation issues appeared at high water percentage limiting their applicability (Figure 1).[18]

In this article, we wish to report on the synthesis and full characterization of a novel family of AIE/ESIPT derivatives based on a bis-imino phenol (anil) motif functionalized by various peripheral substituents (arenes or heteroarenes) bearing electrondonating or electronwithdrawing moieties (Figure 1). This scaffold, derived from Schiff base, is usually obtained in one or two steps from commercially available reagents.[19] The strong H-bonded six-membered ring ensures an efficient ESIPT process but also prevents hydrolysis of the imine bond in aqueous environment, according to a recent study.[20] In order to provide additional examples of AIE/ESIPT dyes with enhanced AIE intensity and emission color fine-tuning, we developed a novel family of bis-anil dyes with additional peripheral arene substitution on the phenolic side.

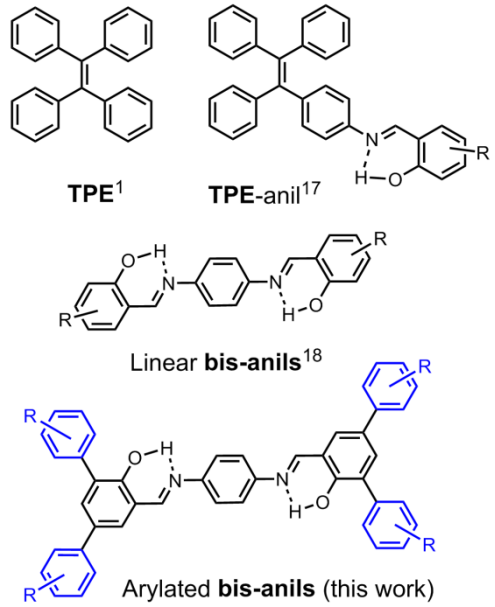

Figure 1. TPE, TPE-anil, linear bis-anils and arylated bis-anils reported herein.

Results and discussion

Bis-anils (**A**) can be prepared in two steps from commercial reagents. 3,5-heteroarene substituted salicylaldehyde derivatives **1-9** are synthesized in one step using Suzuki cross-couplings (Scheme 1). bis-Anils A are then obtained by a condensation in refluxing ethanol with phenylenediamine (Scheme S2). This straightforward method allows for the preparation of a whole series of **A** in multigram scale. All dyes are characterized by ^{1}H, ^{13}C NMR and HR-MS (see the SI). The peripheral substitution of the bis-Anils **A** was easily modified using commercially available boronic acids. Electrodonating groups (EDG) such as OMe or NR_2, electrowithdrawing groups (EWG) such as F, CF_3 or CN but also heteroarenes like thiophenes or pyridines were selected in order to study their AIE behavior and assess the possibility to fine-tune the fluorescence color of the resulting aggregates depending on substitution.

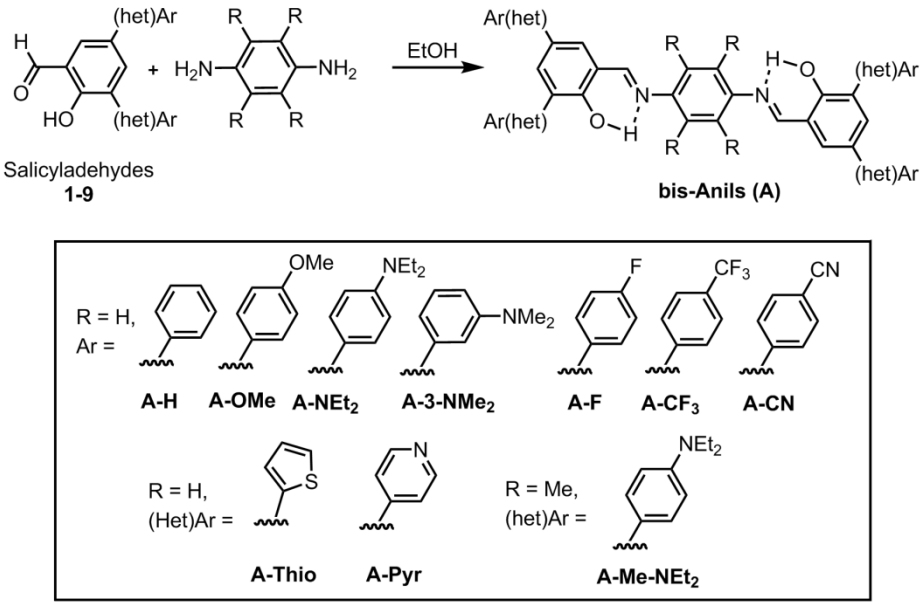

Scheme 1. Synthesis of heteroaryl-Substituted bis-Anil Derivatives (**A**)

Single crystals, suitable for X-ray were obtained for **A-3-NMe$_2$** and **A-Me-NEt$_2$** by recrystallization in a $CHCl_3$/isopropanol mixture. These compounds crystallized in triclinic, P$\bar{1}$ and monoclinic, P21/c space groups, respectively. Their molecular structure confirmed the presence of strong intramolecular O–H…N hydrogen bonds with O–H…N distances of 1.69(2)/1.72(2) Å and 1.80(2) Å and angle values of 158(3)/153(2) °) and 156(3)° respectively and have their imine bond coplanar with the phenol group, which is favorable for the proton transfer process in the excited state. (Figure 2). In the absence of other substituents to the phenol groups, the three phenyl rings compound is planar in the solid state in which the molecules stacked in a parallel fashion to form 1-D columns with short interplanar spacing (3.29 Å). Peripheral substitution at the phenol moieties often breaks this quasi co-planarity,[21] but not systematically.[22] Here, a random molecular arrangement of the peripheral substituents can be observed, revealing a rotor-shaped conformation, for the two dyes.

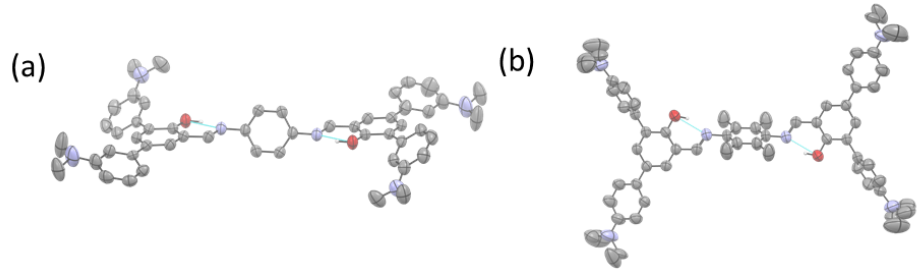

Figure 2. ORTEP diagrams of (a) **A-3-NMe$_2$** (second conformer) and (b) **A-Me-NEt$_2$**. Disorder of substituents is not shown for clarity.

A-3-NMe$_2$ presents in the unit cell two independent conformers around a respective crystallographic centre of inversion: a first conformer with the pair of slightly agitated NMe_2 groups, which displays a

torsion angle of 58.2° between the central ring and the rest of the substituents lying roughly in the same imino-phenol plan. The second conformer looks almost planar, except one pair of NMe_2-substituted arenes clearly out of the mean molecular plane (dihedral angle with the phenol ring of 58.7°); the twist between the central ring and the phenol being only of 6.6°. The planar conformer of **A-3-NMe$_2$** allows columns of limited π-stacking molecules over three levels due to 60° inclination with respect to the elongated molecular axis (distance centroid-centroid between phenol ring and central ring is 3.8 Å) (Figure 3a). This column is surrounded by four columns of the other conformers whose twist prevents aromatic ring overlaps and keep the molecules far away from each other (Figure 3b).

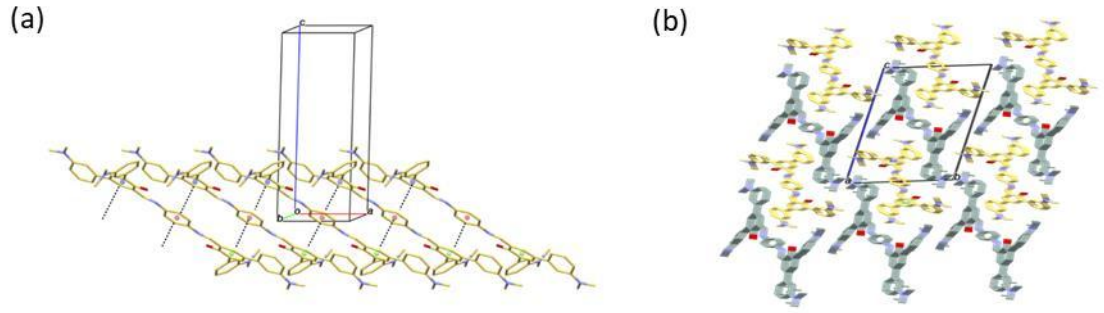

Figure 3. Part of the **A-3-NMe$_2$** crystal assembly down the b crystallographic axis (a) showing column along the a direction of the almost flat conformers (carbons in yellow) along stacking three phenyl rings on top of each other and (b) down the a axis these columns surrounded by four piles without possible π -π stacking of the other conformer (carbons in grey).

Hirshfeld surface analysis and the associated two-dimensional fingerprint plots[23] help to quantify the intermolecular interactions and confirm the contributions to the overall Hirshfeld surface of C–H … π (30.2%), C–H…O and N (6.9%) and π…π (3.4%), highlighting weak face-to-face π–π stacking interactions (Figure S37 and S38).

Methyl tetrasubstitution at the central phenyl ring position, in **A-Me-NEt$_2$** forces a large rotation of 77.8° with the phenol moiety which prevents π-stacking aggregation, a feature propitious for AIE emission. All structural data can be found in the SI.

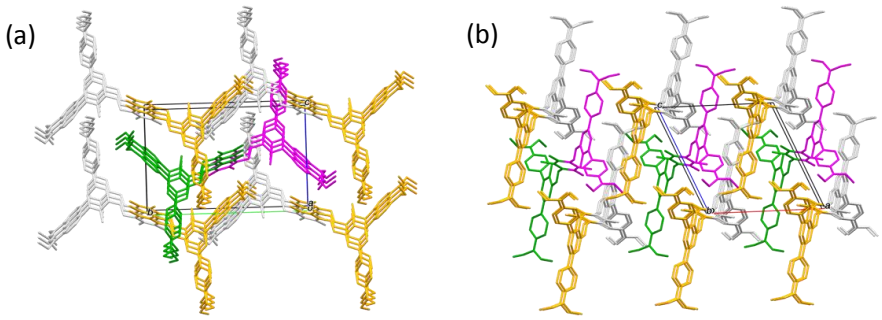

Figure 4. Partial view of the **A-Me-NEt$_2$** crystal packing (a) down the a crystallographic axis and (b) down the b axis. Carbons in grey and golden are the two halves of the molecules formed around an inversion center. In green and magenta are those related to the previous one by crystallographic symmetry elements: a 2-fold axis and a glide mirror, respectively

The photophysical properties of all dyes were first investigated as single molecules in dilute THF solution (Table S2 and Figure 5). All dyes display intense low-energy absorption bands between 388 to 414 nm, with absorption coefficients spanning 9200-34900 $M^{-1}.cm^{-1}$, assigned to the S_0-S_1 transition. Significant differences can be observed in the maximum absorption wavelengths, where the introduction of strong EDG such as amino groups leads to bathochromic shifts (λ_{abs} = 402 nm for **A-Me-NEt$_2$** and 436 nm for **A-4-NEt$_2$**), highlighting a CT nature of this band. Additional intense higher energy bands (observed below 300 nm) can be assigned to the π-π^* transitions of the aromatic rings.

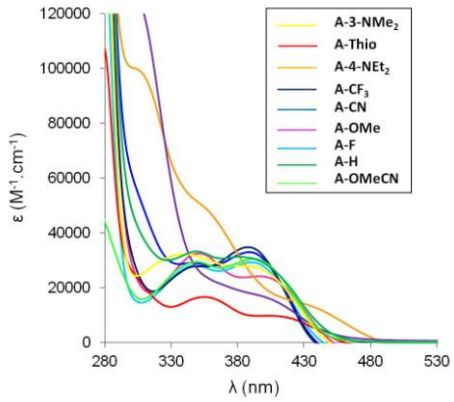

Figure 5. Absorption spectra of all bis-anil dyes **A** in THF (C = 10^{-5}M).

Photoexcitation in the lowest-energy absorption band (λ_{exc} = 385-430 nm), does not lead to the observation of any detectable fluorescence emission in the micromolar concentration range, required for quantum yield calculation. This feature clearly evidences strong fluorescence quenching, due to the numerous rotational and vibrational deactivations on the molecular core, a feature highly beneficial to achieve AIE emission.

The AIE properties of all bis-anils **A** dyes were investigated in THF/H_2O mixtures (Table S2, Figures 6 and S39-S43). **A-H**, **A-OMe**, **A-3-NMe$_2$**, **A-4-NEt$_2$**, **A-F**, **A-CF$_3$** and **A-Me-NEt$_2$** all display strong fluorescence intensity enhancement upon addition of water in THF solutions, from 40% up to 90%, without any sign of precipitation; ascertaining their AIE capacity. The observed emission band can be assigned to the radiative S_1-S_0 transition of the EK^* tautomer, generated upon ESIPT process (see Figure S49 for a schematic representation of excited-state dynamics, and theoretical calculations below). One single quantitative proton transfer, *i.e.* a single EK^* band is observed, which goes in strong contrast with the majority of non-AIE ESIPT dyes where the addition of protic solvent such as ethanol is accompanied by the stabilization of the H-bonded enol tautomer.[24] This difference can be explained by the formation of aggregates which limits the influence of solvatation on the ESIPT process. It is also worth noting that this series of bis-anils AIEgens display a fine-tuning of the maximum emission wavelength, with fluorescence color spanning from orange to near infra-red (NIR) (λ_{em} = 610-715 nm), depending on the electronic nature of the peripheral substitution. **A-H** and EWG-functionalized **A-F** and **A-CF$_3$** are the most hypsochromically shifted AIE compounds in the series (λ_{em} = 610-622 nm), while those with EDG are among the most red-shifted (λ_{em} = 630-715 nm). In addition, the bis anil **A-4-NEt$_2$**, functionalized with the strongest EDG, is the only dye in this series emitting in the NIR region (λ_{em} = 715 nm), highlighting the CT nature of the fluorescence emission of the aggregates. We note that some other examples of ESIPT/AIE emitting in the NIR have been reported.[25]

As exemplified earlier, the nature of the peripheral electronic substitution does influence the fluorescence color, but we also show that the nature of the presence of heteroarene in lieu of arene diminished the AIE capacity of the resulting bis-anil. Indeed, **A-Thio** shows AIE behavior (λ_{em} = 682 nm), up to the addition of 40% water, followed by a strong decrease of fluorescence, attributed to precipitation (Figure S42). **A-Pyr** was not studied, due to strong insolubility issues in THF, at the required concentrations for AIE studies (10^{-5} M). This emphasizes the key role of peripheral arenes in the AIE behaviour of bis-anil derivatives **A**. Interestingly, **A-CN** stands out in the series and shows different photophysical behavior. Indeed, due to its strong EW capacity, the cyano group triggers efficient deprotonation of the phenol moiety in the excited-state, instead of ESIPT, up to the addition of 40% water (Figure 6d). It is well-known that, in the presence of strongly acidic proton, deprotonation can compete with the ESIPT process in the excited-state (Figure S48, and below).[26]

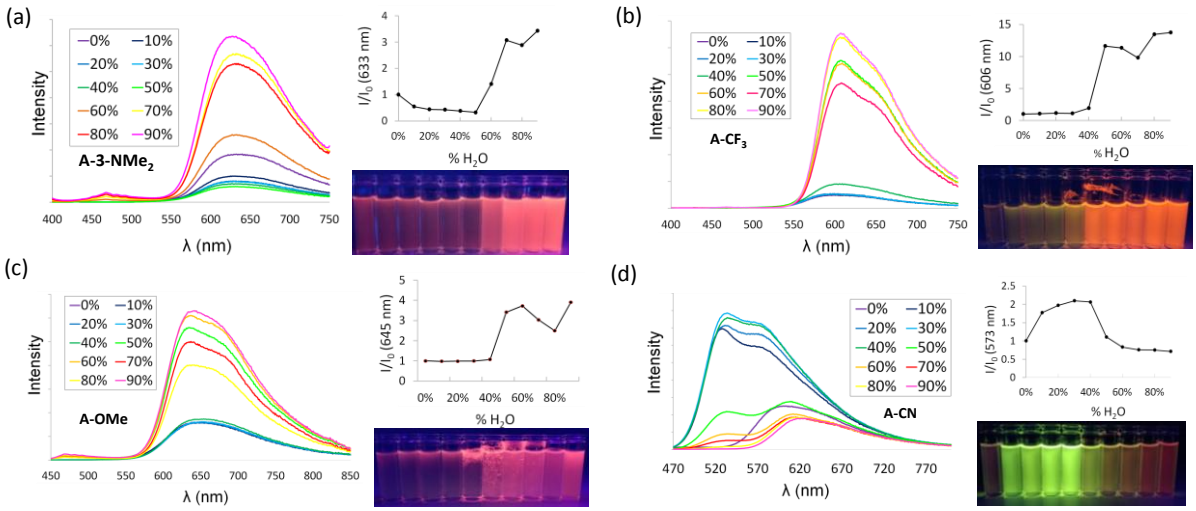

Figure 6. AIE behavior in THF/H_2O mixtures (0% to 90% H_2O) for (a) **A-3-NMe$_2$**, (b) **A-CF$_3$**, (c) **A-OMe** and (d) **A-CN**, at 25°C (0%, purple; 10%, black, 20%, navy blue; 30%, blue; 40%, green; 50%, light green; 60%, orange; 70%, red; 80%, yellow; 90%, pink) (λ_{exc} = 390 nm).

In the case of **A-CN** and according to theory, the resulting fluorescent phenolate, stemming from the mono-deprotonated (ED*) emits at long wavelength whereas the EK* state emits below 600 nm (see calculations below). Therefore the intense green/yellow emission at 573 nm at low water content is likely coming from the EK* species (Figure 6d). Upon further addition of water, this EK* emission band gradually disappears, along with the appearance of a weaker emissive fluorescence band at 605 nm. AIE appears therefore as a process strongly affected by the pKa of the phenolic proton. This dual ED*/EK* emissive process where a proton can be either involved in the ESIPT process or deprotonated in the medium, is highly attractive for the engineering of ratiometric pH sensors based on AIE process. We also recorded the fluorescence emission in the solid-state, as powders of all dyes (Figure S44 and table S2). The emission wavelengths are in the same range as those observed in aggregates (λ_{em} = 613-728 nm), highlighting the presence of the EK* band in the solid-state as well. **A-CN** presents only one band at 635nm, possibly also corresponding to the ED* excited form. The quantum yield, calculated as absolute, are weak, peaking at 11% for **A-H**.

In order to enhance the fluorescence intensity of the red-shifted EK* band, while maintaining the possibility to observe deprotonation, an additional bis-anil derivative, **A-OMeCN** was synthesized (Scheme 2). Salicylaldehyde **5** was first refluxed with an excess of phenylenediamine to yield an aniline intermediate, which was further condensed with one equivalent of 3,5-dibenzonitrile-salicyladehyde **1**. Bis-anil **A-OMeCN**, which was obtained after purification on column chromatography in 16% yield, incorporates two different imine moieties, with methoxy groups on one side and cyano groups on the other side (Scheme 2). The AIE behavior of **A-OMeCN** was studied in

THF/H_2O mixtures, at different pH values in order to investigate the possibility to obtain pH-sensitive AIE dyes (Figure 7 and S45-47).

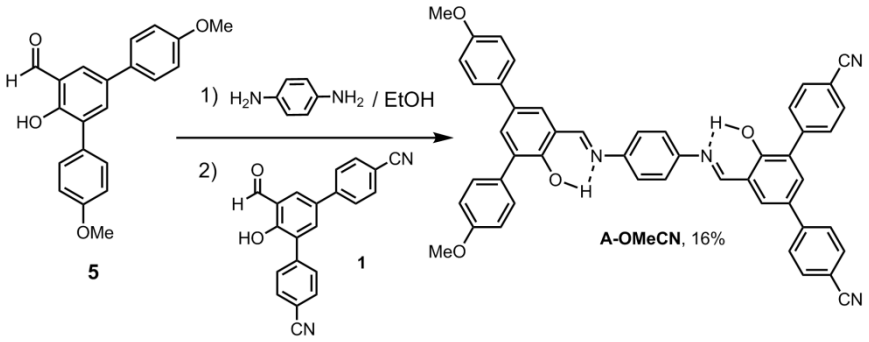

Scheme 2. Synthesis of bis-anil **A-OMeCN.**

At pH 1.8, gradual addition of water in THF solutions of **A-OMeCN** (C = 10^{-5}M) leads to the gradual appearance of a red fluorescence, translating into a single EK* band at 636 nm, consistent with the absence of deprotonation in strong acidic conditions (Figure 7a). At pH 7.4, a significantly different behavior is observed, *i.e.*, a first intense emission band appears upon addition of water, in the green region at 536 nm, which could be attributed to the monodeprotonation of one phenol moiety on the imino-phenol scaffold.

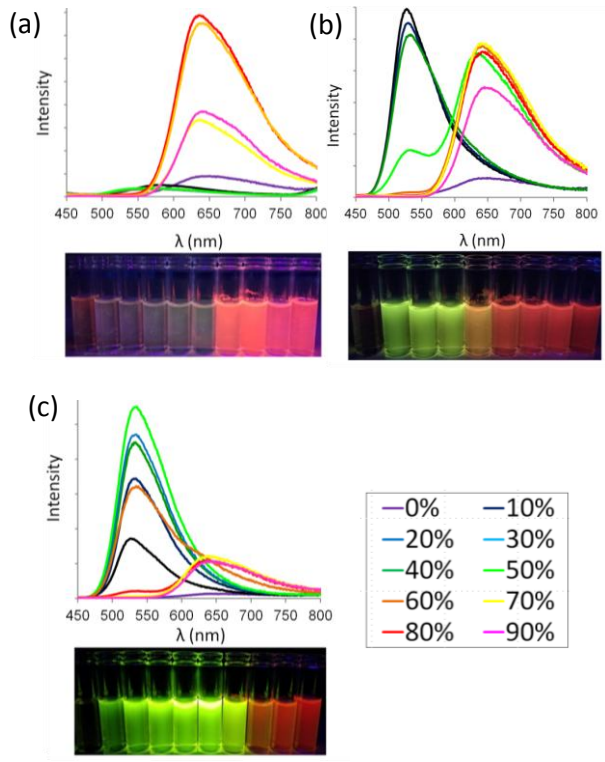

Figure 7. (a) AIE behavior in THF/H_2O mixtures (0% H_2O to 90% H_2O) of **A-OMeCN** at (a) pH 1.8, (b) pH 7.4 and (c) pH 11.3, at 25°C. (0%, purple; 10%, black, 20%, navy blue; 30%, blue; 40%, green; 50%, light green; 60%, orange; 70%, red; 80%, yellow; 90%, pink) (λ_{exc} = 390 nm).

This emissive anionic derivative (Fig. 6, see also calculations) is observed up to the addition of 60% of water. Upon further increase of water percentage, a slow decrease of the band at 536 nm, accompanied by the gradual appearance of a red-emitting band at 636 nm are recorded (Figure 7b). The latter band, in the red region is consistent with the one observed at acidic pH and can likely be ascribed to the decay of the EK^* tautomer. At basic pH, where deprotonation is logically favored, an intense anionic band is recorded up to 70% water. It is worth noting that even in strongly basic conditions (pH 11.3), the presence of the emission at 636 nm is observed, consistent with the formation of aggregates where deprotonation seems to be no longer possible. This does corroborate the fact that aggregation limits the influence of solvatation and more generally protects AIE dyes from variation of their local environments. This pH sensitivity in **A-OMeCN** is clearly observed at 60% water in THF where a dual emission with different intensity ratios between the two fluorescence bands is observed at pH values 10.3 and 11.3 (Figure S47 left). At 90% water in THF, **A-OMeCN** solely emits in the red at 636 nm, regardless of the value of the pH (Figure S47 right).

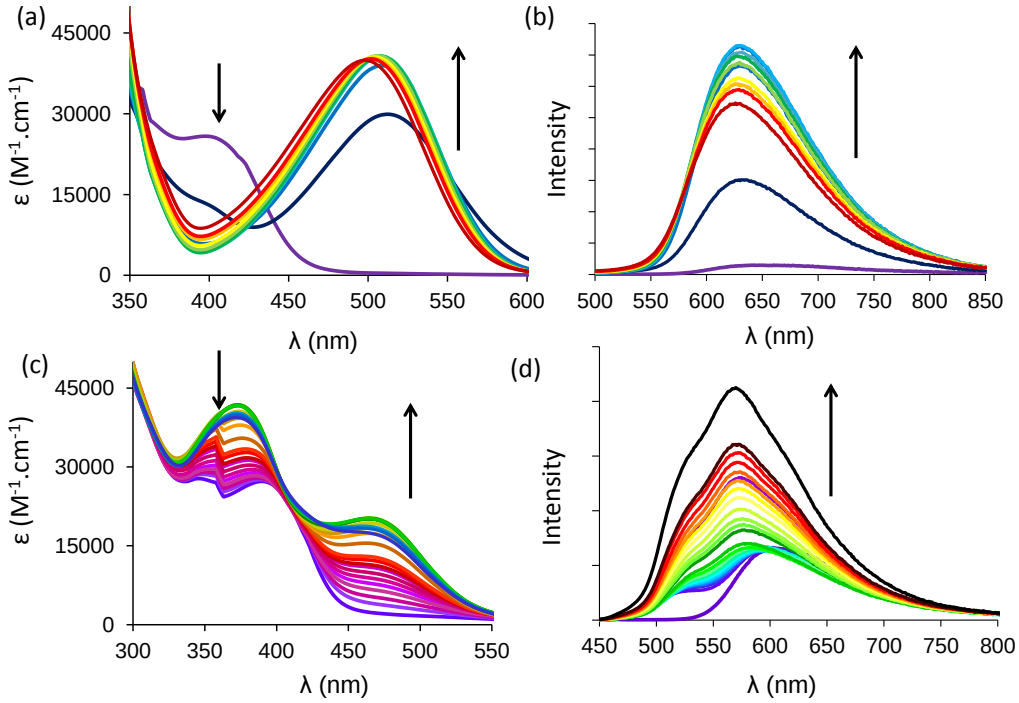

Figure 8. . Overlay of absorption (a) (c) and emission (b) (d) spectra of bis-anil **A-OMe** (top) and **A-CN** (bottom) in THF recorded after successive addition of increasing equivalents of Bu_4NOH (a) (b) and 1,8-diazabicyclo(5.4.0)undec-7-ene (DBU) (c) (d), at 25°C.

To shed more light on the nature of the transition, basic titrations in absorption and emission were performed on two representative dyes, namely **A-OMe** and **A-CN**, upon addition of increasing equivalents of tetrabutylammonium hydroxide (Bu_4NOH) or 1,8-diazabicyclo(5.4.0)undec-7-ene

(DBU) in THF (Figure 8). In absorption, addition of base leads to a progressive decrease of the band corresponding to the neutral species (around 390 nm) and a concomitant increase of a new band centered around 480 nm, which can be ascribed to the *in situ* formation of anionic species. Two isobestic are observed at 432 and 407 nm for **A-OMe** and **A-CN**, respectively. Photoexcitation at these isobestic points triggers an increase of the fluorescence intensity in both cases. For **A-OMe**, the monoanionic excited species ED^* is observed at 628 nm, while for **A-CN**, a blue-shifted band is recorded at 570 nm. The nature of this latter band remains unclear and could be possibly attributed to the DD^* transition, as calculations predict ED^* above 600 nm, but a DD^* at 558 nm (see below).

To gain more insights into the aggregation processes for the two different excited-states observed, dynamic light-scattering (DLS) experiments were conducted (Figure S48) on **A-OMeCN** at 90% H_2O in THF. Interestingly, large particle sizes of 319 nm and 351 nm were recorded for **A-OMeCN** at 636 nm at acidic or basic pH (1.8 and 11.3), respectively. At 536 nm, in basic conditions (pH 11.3), no particle were observed during DLS experiments, highlighting the fact that the anionic species do not undergo AIE process, unlike their neutral counterparts.

We have also performed DFT and TD-DFT calculations (in THF) for three representative systems, namely **A-OMe**, **A-CN**, and **A-OMeCN** to gain more information regarding the possible nature of the emissive species (see the SI for computational details). For **A-OMe** in its neutral form, TD-DFT predicts that the EK^* tautomer is more stable by -0.26 eV on the free energy scale as compared to the initially excited EE^* form, which indicates quantitative proton transfer, according to previous calculations performed using a similar level of theory.[27] In contrast, in this system, like in the two others investigated with theory, the double-ESIPT structure (KK^*) is less stable than EK^* (by 0.08 eV for **A-OMe**), hinting that the redshifted emission noted experimentally at 642 nm (Fig. 5c) likely comes from the EK^* tautomer only. The mixed coupled-cluster/TD-DFT protocol used for vertical transition energies returns a vertical emission at 608 nm for EK^*, in good agreement with experiment ($|\Delta|$=0.11 eV). According to theory, the mono-deprotonated **A-OMe** species, ED^*, would emit at an even longer wavelength (720 nm), whereas the EE^* tautomer would emit at 486 nm, which is clearly not compatible with the measurements. In short, it seems plausible that the observed fluorescence of **A-Ome** originates from the EK^* structure. In **A-CN**, theory also predicts that EK^* is more stable than KK^* (Table S3) and that its vertical fluorescence appears at 560 nm (Table S4), again compatible with the experimental value (573 nm, see Fig. 6d). The mono-deprotonated species, ED^* is the only tautomer predicted by theory to fluoresce above 600 nm (630 nm), explaining why we attributed the most redshifted band in Fig. 6d to this structure. Indeed the doubly-depronotated DD^* species vertical emission is given at 558 nm by the selected approach. Finally for **A-OMeCN**, theory predicts that the most stable neutral tautomer in the excited state is the KE^* form (in which ESIPT takes place on the

OMe "side") with a vertical emission estimated at 612 nm (Tables S3 and S4), a value consistent with experiment (636 nm, see Fig. 7a). Interestingly the mono-deprotonated species, ED^* (with the anion on the CN "side") is predicted by theory to emerge at almost the same wavelength (616 nm, see Table S4), whereas the fully deprotonated species would emit at 565 nm. We therefore tentatively attribute the experimental emission at 536 nm in the **A-OMeCN** spectra to this dianionic species, whereas at low pH (Fig. 7c), it is honestly difficult to determine if the relatively low-intense band above 600 nm originates from the KE^* or ED^* species or a mixture of the two.

In conclusion, we have designed, synthesized and characterized a whole new family of ESIPT/AIE fluorophores, whose fluorescence color can be finely tuned by modification of the electronic nature of the peripheral substitution, highlighting a CT-controlled emission. Single crystal X-rays reveal a rotor-shaped conformation of these dyes and weak face-to-face π–π stacking interactions. Moreover, we have evidenced a deprotonation process which can compete with ESIPT when the acidity of the phenolic proton is enhanced by introduction of EWG such as cyano. This leads to a pH sensitivity of the emission profile with a dual emission in neutral to basic pH. Future work will focus on the possibility to probe small pH modifications *in cellulo*.

Experimental section

CCDC deposit number: 2187876 (for **A-3-NMe_2**) and 2190380 (for **A-Me-NEt_2**).

Salicylaldehydes **3, 4 ,5** and **9** are already described in the literature[28,29]

General procedure for the synthesis of salicylaldehydes 1-9:
3,5-diiodoalicylaldehyde (0.1 mmol.), the corresponding boronic acid (0.3 mmol.), potassium carbonate (0.4 mmol.) and bis(triphenylphosphine)palladium(II) dichloride (5 mol. %) are dried under vaccum in a shlenck tube under argon atmosphere. 1,4-dioxane/H_2O, 4:1 was degassed with argon for 15 minutes, before it was syringed onto the solids. The resulting mixture was stirred for 15 hours at 95°C. The reaction was then quenched with 2M HCl solution. The crude product was extracted three times with ethyl acetate and the organic layers were washed with brine, dried with $MgSO_4$ before the solvents were removed *in vacuo*. The crude product was purified by a silica column chromatography to yield salicylaldehydes **1-9**.
Salicylaldehyde 1. 52%. Pet. Ether/EtOAc 10:0 to 8:2. Pale yellow solid. ^{1}H NMR (500 MHz, $CDCl_3$) δ 11.71 (s, 1H), 10.07 (s, 1H), 7.86 (d, ^4J = 2.4 Hz, 1H), 7.83 (d, ^3J = 2.4 Hz, 1H), 7.80-7.74 (m, 6H), 7.72-7.68 (m, 2H). $^{13}C\{^1H\}$NMR (126 MHz, $CDCl_3$) δ 196.7, 159.2, 143.4, 140.58, 136.1, 133.1, 132.7, 132.4, 131.7, 130.2, 129.7, 127.4, 121.4, 112.0, 111.7, 77.4, 77.2, 76.9. HRMS (ESI-TOF) m/z: [M+H] Calcd for $C_{21}H_{12}N_2O_2$: 324.0893, Found: 324.0890.

Salicylaldehyde 2. 48%. Pet. Ether/EtOAc 10:0 to 8:2. Yellow solid. ^{1}H NMR (500 MHz, $CDCl_3$) δ 11.64 (s, 1H), 10.07 (s, 1H), 7.87-7.84 (m, 2H), 7.79 -7.69 (m, 8H). $^{13}C\{^{1}H\}$NMR (126 MHz, $CDCl_3$) δ 196.8, 159.0, 142.6, 139.7, 136.4, 132.3, 132.2, 130.3, 130.1, 130.1, 129.8, 127.1, 126.3, 126.2, 126.2, 126.2, 125.5, 125.5, 125.5, 125.4, 123.2, 121.3. ^{19}F NMR (471 MHz, $CDCl_3$) δ -62.5, -62.6. HRMS (ESI-TOF) m/z: [M+H] Calcd for $C_{21}H_{12}F_6O_2$: 410.0736; Found : 410.0735.

Salicylaldehyde 3.[28] 71%. Pet. Ether/EtOAc 10:0 to 8:2. Yellow solid. ^{1}H NMR (500 MHz, $CDCl_3$) δ 11.52 (s, 1H), 10.03 (s, 1H), 7.76 (d, ^{4}J = 2.3 Hz, 1H), 7.72 (d, ^{4}J = 2.4 Hz, 1H), 7.65-7.59 (m, 2H), 7.57-7.51 (m, 2H), 7.20-7.13 (m, 4H). $^{13}C\{^{1}H\}$NMR (126 MHz, $CDCl_3$) δ 196.9, 163.5, 161.6, 158.1, 136.3, 135.4, 132.5, 131.2, 131.1, 131.0, 130.1, 128.4, 128.3, 121.0, 116.1, 115.9, 115.5, 115.3. ^{19}F NMR (471 MHz, $CDCl_3$) δ -114.1, -115.0

Salicylaldehyde 4.[28] 79%. Pet. Ether/EtOAc 10:0 to 9:1. Yellow solid. ^{1}H NMR (500 MHz, $CDCl_3$) ^{1}H NMR (500 MHz, $CDCl_3$) δ 11.52 (s, 1H), 10.04 (s, 1H), 7.87 (d, ^{4}J = 2.4, 1H), 7.77 (d, ^{4}J = 2.4 Hz, 1H), 7.67-7.63 (m, 2H), 7.62-7.59 (m, 2H), 7.51-7.45 (m, 4H), 7.44-7.35 (m, 2H). $^{13}C\{^{1}H\}$NMR (126 MHz, $CDCl_3$) δ 197.0, 158.3, 139.4, 136.7, 136.3, 133.4, 131.3, 131.1, 129.4, 129.1, 128.4, 127.9, 127.5, 126.7, 121.1.

Salicylaldehyde 5.[28] 79%. Pet. Ether/EtOAc 10:0 to 8:2. Yellow solid. ^{1}H NMR (500 MHz, $CDCl_3$) ^{1}H NMR (500 MHz, $CDCl_3$) δ 11.46 (s, 1H), 10.01 (s, 1H), 7.79 (d, ^{4}J = 2.4 Hz, 1H), 7.67 (d, ^{4}J = 2.4 Hz, 1H), 7.62 -7.57 (m, 2H), 7.55-7.49 (m, 2H), 7.05-6.98 (m, 3H), 3.87 (s, 3H), 3.86 (s, 3H). $^{13}C\{^{1}H\}$ NMR (126 MHz, $CDCl_3$) δ 197.1, 159.4, 159.4, 157.9, 136.2, 133.2, 132.1, 130.7, 130.6, 130.4, 128.8, 127.9, 121.1, 114.6, 114.0, 55.5, 55.5.

Salicylaldehyde 6. 41%. Pet. Ether/EtOAc 10:0 to 7:3. Yellow solid. ^{1}H NMR (500 MHz, $CDCl_3$) ^{1}H NMR (500 MHz, $CDCl_3$) δ 11.39 (s, 1H), 9.99 (s, 1H), 7.81 (d, ^{4}J = 2.4 Hz, 1H), 7.60 (d, ^{4}J = 2.4 Hz, 1H), 7.56-7.51 (m, 2H), 7.48-7.44 (m, 2H), 6.80-6.73 (m, 4H), 3.41 (q, ^{3}J = 7.1 Hz, 8H), 1.21 (t, J = 7.1 Hz, 12H). $^{13}C\{^{1}H\}$NMR (126 MHz, $CDCl_3$) δ 197.3, 157.5, 147.4, 147.3, 137.9, 135.4, 133.6, 131.1, 130.4, 129.0, 127.6, 126.6, 123.2, 121.1, 114.2, 112.2, 111.5, 77.4, 77.4, 77.2, 76.9, 44.6, 44.5, 12.8, 12.7. HRMS (ESI-TOF) m/z: [M+H] Calcd for $C_{27}H_{33}N_2O_2$: 417.2537; Found: 417.2531.

Salicylaldehyde 7. 81%. Pet. Ether/EtOAc 10:0 to 7:3. Yellow solid. ^{1}H NMR (500 MHz, $CDCl_3$) ^{1}H NMR (500 MHz, CD_2Cl_2) δ 11.45 (s, 1H), 10.02 (s, 1H), 7.90 (d, ^{4}J = 2.4 Hz, 1H), 7.79 (d, ^{4}J = 2.4 Hz, 1H), 7.31 (td, ^{3}J = 7.9 Hz, ^{4}J = 2.2 Hz, 2H), 6.99-6.97 (m, 1H), 6.97-6.93 (m, 2H), 6.93-6.91 (m, 1H), 6.78 (dd, ^{3}J = 8.4 Hz, ^{4}J =2.7 Hz, 1H), 6.75 (dd, ^{3}J =8.4 Hz, ^{4}J =2.7 Hz, 1H), 3.00 (s, 6H), 2.98 (s, 6H). $^{13}C\{^{1}H\}$NMR (126 MHz, CD_2Cl_2) δ 197.7, 158.5, 151.6, 151.1, 140.6, 137.6, 137.0, 134.4, 132.0, 131.6, 130.0, 129.2, 121.33, 118.1, 115.3, 114.1, 112.3, 112.1, 111.1, 40.8. HRMS (ESI-TOF) m/z: [M+H] Calcd for $C_{23}H_{25}N_2O_2$: 361.1911; Found: 361.1913.

Salicylaldehyde 8. 53%. Pet. Ether/EtOAc 10:0 to 8:2. Red solid. ^{1}H NMR (500 MHz, $CDCl_3$) δ 11.89 (s, 1H), 9.96 (s, 1H), 8.08 (d, ^{4}J = 2.3 Hz, 1H), 7.70-7.66 (m, 2H), 7.41 (dd, ^{3}J = 5.2 Hz, ^{4}J = 1.2 Hz, 1H), 7.31 (dd, ^{3}J = 5.2 Hz, ^{4}J = 1.2 Hz, 1H), 7.29 (dd, ^{3}J = 3.6 Hz, ^{4}J = 1.2 Hz, 1H), 7.15 (dd, ^{3}J =5.2 Hz, ^{4}J = 3.6 Hz, 1H), 7.11 (dd, ^{3}J =5.2 Hz, ^{4}J = 3.6 Hz, 1H). $^{13}C\{^{1}H\}$NMR (126 MHz, $CDCl_3$) δ 196.9,

157.4, 142.4, 137.2, 133.0, 129.8, 128.3, 127.5, 127.1, 127.1, 126.4, 125.1, 124.2, 123.3, 121.2. HRMS (ESI-TOF) m/z: [M+H] Calcd for $C_{15}H_{11}O_2S_2$: 287.0195; Found: 287.0178.

Salicylaldehyde 9.[29] 62%. $CHCl_3$/EtOH (99:1). Yellow powder. ^{1}H NMR (500 MHz, ^{6}d -DMSO) δ 11.57 (br, 1H), 10.21 (s, 1H), 8.70 -8.68 (m, 2H), 8.67-8.65 (m, 2H), 8.40 (d, ^4J = 2.4 Hz, 1H), 8.20 (d, ^4J = 2.4 Hz, 1H), 7.88-7.84 (m, 2H), 7.77-7.72 (m, 2H). ^{13}C{^{1}H} NMR (126 MHz, ^{6}d -DMSO) δ 197.1, 158.4, 150.3, 149.6, 145.2, 143.5, 135.3, 132.6, 129.1, 127.8, 124.1, 122.1, 120.8. HRMS (ESI-TOF) m/z: [M+H] Calcd for $C_{17}H_{13}N_2O_2$: 277.0972; Found: 277.0964.

General procedure for the synthesis of bis-anils A

Salicylaldehyde 1-9 are first solubilized in a minimum amount of hot ethanol at 65°C. p-Phenylenediamine is then added and the solution stirred at 80°C for 1,5 hours. The crude mixture is centrifuged and the obtained precipitate is washed with cold ethanol to yield the desired **bis-anil A**.

Bis-anil A-H. 82%. Orange/red solid. ^{1}H NMR (500 MHz, $CDCl_3$) δ 13.92 (s, 2H), 8.83 (s, 2H), 7.74 (d, ^{4}J = 2.3 Hz, 2H), 7.73-7.70 (m, 4H), 7.65 (d, ^{4}J = 2.3 Hz, 2H), 7.64-7.61 (m, 4H), 7.52-7.44 (m, 8H), 7.41 (s, 4H), 7.40-7.33 (m, 4H). ^{13}C{^{1}H} NMR (126 MHz, $CDCl_3$) δ 162.5, 158.2, 147.0, 140.2, 137.6, 133.3, 132.6, 130.8, 130.2, 129.6, 129.1, 128.4, 127.6, 127.2, 126.8, 122.5, 119.6, 77.4, 77.2, 76.9. HRMS (ESI-TOF) m/z: [M+H] Calcd for $C_{21}H_{12}N_2O_2$: 621.2537, Found: 621.2535.

Bis-anil A-OMe. 80%. Orange/red solid. ^{1}H NMR (500 MHz, $CDCl_3$) δ 13.71 (s, 2H), 8.66 (s, 2H), 7.56-7.49 (m, 6H), 7.43-7.36 (m, 6H), 7.13 (s, 2H), 6.89 (d, ^3J = 8.8 Hz, 4H), 6.86 (d, ^3J = 8.8 Hz, 4H), 3.74 (s, 6H), 3.73 (s, 6H). ^{13}C{^{1}H} NMR (126 MHz, $CDCl_3$) δ 162.6, 159.2, 159.1, 157.7, 147.0, 132.9, 132.7, 132.3, 130.7, 130.3, 130.0, 129.3, 127.8, 122.5, 119.6, 114.5, 113.9, 55.5, 55.5. HRMS (ESI-TOF) m/z: [M+H] Calcd for $C_{48}H_{40}N_2O_6$: 740.2855, Found: 740.2881.

Bis-anil A-NEt$_2$. 72%. Orange/red solid. ^{1}H NMR (500 MHz, $CDCl_3$) δ 13.71 (s, 2H), 8.79 (s, 2H), 7.68 (d, ^4J = 2.3 Hz, 2H), 7.59 (d, ^3J = 8.9 Hz, 4H), 7.52-7.45 (m, 6H), 7.39 (s, 4H), 6.79 (d, ^3J = 8.9 Hz, 4H), 6.76 (d, ^3J = 8.9 Hz, 4H), 3.41 (qd, ^3J = 7.1 Hz, ^4J = 4.6 Hz, 16H), 1.21 (td, ^3J = 7.0 Hz, ^4J = 2.5 Hz, 24H). ^{13}C{^{1}H} NMR (126 MHz, $CDCl_3$) δ 162.9, 157.2, 147.2, 147.2, 147.0, 132.7, 132.1, 130.7, 130.4, 128.0, 127.6, 127.5, 124.6, 122.4, 119.4, 112.2, 111.6, 44.6, 44.6, 12.9, 12.8. HRMS (ESI-TOF) m/z: [M+H] Calcd for $C_{60}H_{69}N_6O_2$: 905.5477, Found: 905.5468.

Bis-anil A-3NMe$_2$. 83%. Orange/red solid. ^{1}H NMR (500 MHz, $CDCl_3$) δ 13.83 (s, 2H), 8.82 (s, 2H), 7.78 (d, ^4J = 2.3 Hz, 2H), 7.64 (d, ^4J = 2.3 Hz, 2H), 7.40 (s, 4H), 7.39-7.30 (m, 4H), 7.09-7.03 (m, 4H), 6.98 (d, ^4J = 8.3 Hz, 2H), 6.94 (s, 2H), 6.80 (dd, ^3J = 8.3 Hz, ^4J =2.4 Hz, 2H), 6.76 (dd, ^3J = 8.3 Hz, ^4J = 2.6 Hz, 2H), 3.03 (s, 12H), 3.01 (s, 12H). ^{13}C{^{1}H} NMR (126 MHz, $CDCl_3$) δ 162.6, 158.1, 151.2, 150.8, 147.0, 141.3, 138.5, 133.5, 133.4, 131.5, 130.1, 129.7, 129.0, 122.5, 119.4, 118.1, 115.4, 114.0, 112.0, 111.5, 111.1, 40.9, 40.9. HRMS (ESI-TOF) m/z: [M+H] Calcd for $C_{52}H_{53}N_6O_2$: 793.4225, Found: 793.4236.

Bis-anil A-F.[30] 71%. Orange/red solid. ^{1}H NMR (500 MHz, $C_2D_2Cl_4$) δ 13.97 (s, 2H), 8.83 (s, 2H), 7.74 – 7.69 (m, 4H), 7.67-7.62 (m, 4H), 7.62 -7.55 (m, 4H), 7.44 (s, 4H), 7.25-7.15 (m, 8H). ^{19}F NMR

(471 MHz, $C_2D_2Cl_4$) δ -114.4, -115.2. HRMS (ESI-TOF) m/z: [M+H] Calcd for $C_{44}H_{29}F_4N_2O_2$: 693.2160, Found: 693.2146.

Bis-anil A-CF$_3$.[30] 83%. Orange/red solid. ^{1}H NMR (500 MHz, $CDCl_3$) δ 14.14 (s, 2H), 8.87 (s, 2H), 7.83 (d, ^3J = 8.1 Hz, 4H), 7.78-7.69 (m, 16H), 7.45 (s, 4H). ^{19}F NMR (471 MHz, $CDCl_3$) δ -62.4, -62.5. HRMS (ESI-TOF) m/z: [M+H] Calcd for $C_{48}H_{29}F_{12}N_2O_2$: 893.2032, Found: 893.2044.

Bis-anil A-CN.[30] 85%. Orange/red solid. ^{1}H NMR (500 MHz, $C_2D_2Cl_4$) δ 14.31 (s, 2H), 8.87 (s, 2H), 7.87 (d, ^3J = 8.4 Hz, 4H), 7.83-7.69 (m, 16H), 7.47 (s, 4H). HRMS (ESI-TOF) m/z: [M+H] Calcd for $C_{48}H_{29}N_6O_2$: 721.2347, Found: 721.2331.

Bis-anil A-Thio.[30] 85%. Orange/red solid. ^{1}H NMR (500 MHz, $CDCl_3$) δ 14.45 (s, 2H), 8.80 (s, 2H), 8.01 (d, ^3J = 2.3 Hz, 2H), 7.72 (dd, ^3J= 3.7 Hz, ^4J = 1.2 Hz, 2H), 7.60 (d, ^4J = 2.3 Hz, 2H), 7.46 (s, 4H), 7.42 (dd, ^3J= 5.2 Hz, ^4J = 1.2 Hz, 2H), 7.32-7.27 (m, 4H), 7.17 (dd, ^3J = 5.2 Hz, ^4J = 3.7 Hz, 2H), 7.11 (dd, J = 5.2, 3.7 Hz, 2H). HRMS (ESI-TOF) m/z: [M+H] Calcd for $C_{36}H_{25}N_2O_2S_4$: 645.0793, Found: 645.0782.

Bis-anil A-Pyr.[30] 61%. Orange/red solid. ^{1}H NMR (500 MHz, $C_2D_2Cl_4$) δ 14.40 (s, 2H), 8.88 (s, 2H), 8.75-8.69 (m, 4H), 8.71-8.65 (m, 4H), 7.86-7.78 (m, 4H), 7.72-7.67 (m, 4H), 7.60-7.56 (m, 4H), 7.49 (s, 4H). HRMS (ESI-TOF) m/z : [M+H] Calc. for $C_{40}H_{29}N_6O_2$: 625.2347, Found: 625.2363.

Bis-anil A-Me-NEt$_2$. 58%. Orange/red solid. ^{1}H NMR (500 MHz, $CDCl_3$) δ 13.54 (s, 2H), 8.38 (s, 2H), 7.70 (d, ^4J = 2.4 Hz, 2H), 7.63 (d, ^3J = 8.9 Hz, 4H), 7.48 (d, ^3J = 8.9 Hz, 4H), 7.42 (d, ^4J = 2.4 Hz, 2H), 6.80 (d, ^3J = 8.9 Hz, 4H), 6.76 (d, ^3J = 8.9 Hz, 4H), 3.41 (q, ^3J = 7.1 Hz, 16H), 2.18 (s, 12H), 1.21 (td, ^3J = 7.0 Hz, ^4J = 4.3 Hz, 24H). ^{13}C NMR (126 MHz, $CDCl_3$) δ 168.1, 157.2, 147.2, 147.0, 146.1, 132.7, 131.8, 130.7, 130.5, 128.0, 127.6, 127.6, 125.3, 124.5, 119.1, 112.2, 111.6, 44.6, 44.5, 15.5, 12.9, 12.8. HRMS (ESI-TOF) m/z: [M+H] Calcd for $C_{64}H_{77}N_6O_2$: 961.6103, Found: 961.6058.

Synthesis of Bis-anil A-OMeCN. p-Phenylenediamine (27 mg, 0.25 mmol.) is solubilized in 70 mL of hot ethanol (60°C). Salicylaldehyde **5** (84 mg, 0.25 mmol.), solubilized in 70 mL of hot ethanol (60 °C) is added dropwise to the p-phenylenediamine solution. The resulting mixture is stirred for 30 minutes at 70 °C, before salicylaldehyde **1** (81 mg, 0.25 mmol.) is added and the mixture stirred for another 1.5 hours at 70 °C. The mixture is then warmed up to room temperature and around half of the ethanol is removed under vacuum. The resulting crude solid is then washed with ethanol, centrifugated and purified with silica gel chromatography (CH_2Cl_2/ EtOAc: 10/0 to 8/2) to afforded **bis-anil A-OMeCN** as red powder (29 mg, 16 %). ^{1}H NMR (500 MHz, $CDCl_3$) δ 14.36 (s, 1H), 13.76 (s, 1H), 8.84 (s, 1H), 8.81 (s, 1H), 7.85-7.50 (m, 16H), 7.42 (s, 4H), 7.03 (d, ^3J = 8.4 Hz, 2H), 7.00 (d, ^3J = 8.2 Hz, 2H), 3.88 (s, 3H), 3.86 (s, 3H). ^{13}C NMR (126 MHz, $CDCl_3$) δ 163.0, 161.6, 159.3, 159.2, 159.2, 157.7, 147.6, 146.0, 144.2, 141.9, 133.0, 132.9, 132.8, 132.6, 132.4, 132.3, 131.4, 130.6, 130.4, 130.2, 130.0, 129.4, 129.2, 127.8, 127.3, 122.7, 122.6, 120.1, 119.5, 119.1, 118.9, 114.5, 113.9, 111.4, 111.1, 55.5, 55.5. HRMS (ESI-TOF) m/z: [M+H] Calcd for $C_{48}H_{35}N_4O_4$: 731.2653, Found: 731.2641.

Acknowledgments

The authors thank the CNRS for financial support. T.S. acknowledges the ministère de l'enseignement supérieur et de la recherche for a PhD fellowship. This work of the Interdisciplinary Institute HiFunMat, as part of the ITI 2021-2028 program of the University of Strasbourg, CNRS and Inserm, was supported by IdEx Unistra (ANR-10-IDEX-0002) and SFRI (STRAT'US project, ANR-20-SFRI-0012) under the framework of the French Investments for the Future Program. D.J. thanks the CCIPL (Centre de Calcul Intensif des Pays de la Loire) installed in Nantes for generous allocation of computational time.

Keywords: Aggregation-induced Emission - ESIPT - Fluorescence- pH - Schiff base

References

1 (a) J. Luo, Z. Xie, J. W. Lam, L. Cheng, H. Chen, C. Qiu, H. S. Kwok, X. Zhan, Y. Liu, D. Zhu and B.Z. Tang, *Chem. Commun*., **2001**, 1740. (b) J. Mei, N. L. Leung, R. T. Kwok, J. W. Lam, B.Z. Tang, *Chem. Rev*. **2015**, 115, 11718. (c) Z. Zhao, H. Zhang, J.W.Y. Lam, B.Z. Tang, *Angew. Chem., Int. Ed*., **2020**, 59, 9888.

2 H.-T. Feng, Y.-X. Yuan, J.-B. Xiong, Y.-S. Zheng B.Z. Tang, *Chem. Soc. Rev*., **2018**, 47, 7452.

3 P. Shen, Z. Zhuang, Z. Zhao, B.Z. Tang, *J. Mater. Chem. C*, **2018**, 6, 11835.

4 J. Li, J. Wang H. Li, N. Song, D. Wang, B.Z. Tang, *Chem. Soc. Rev*., **2020**, 49, 1144.

5 (a) J. Zhao, S. Ji, Y. Chen, H. Guo, P. Yang, *Phys. Chem. Chem. Phys*., **2012**, 14, 8803. (b) J. Massue, D. Jacquemin, G. Ulrich, *Chem. Lett*., **2018**, 47, 9, 1083-1089. (c) T. Stoerkler, T. Pariat, A.D. Laurent, D. Jacquemin, G. Ulrich, J. Massue, *Molecules*, **2022**, 27, 2443.

6 (a) V.S. Padalkar, S. Seki, *Chem. Soc. Rev*., **2016**, 45, 169. (b) X. Liu, A. Li, W. Xu, Z. Ma, X. Jia, *Mater. Chem. Front*., **2019**, 3, 620. (c) V. Mishra, C. Ghanavatkar, N. Sekar, *Chemistryselect*, **2020**, 5, 2103. (d) M.K. Bera, P. Pal, S. Malik, *J. Mater. Chem. C*, **2020**, 8, 788. (e) H. Hu, X. Cheng, Z. Ma, R.P. Sijbesma, Z. Ma, *J. Am. Chem. Soc*., **2022**, 144, 22, 9971.

7 (a) Q. Chen, C. Jia, Y. Zhang, W. Du, Y. Wang, Y. Huang, Q. Yanga, Q. Zhang, *J. Mater. Chem. B*, **2017**, 5, 7736. (b) H.-W. Zheng, Y. Kang, M. Wu, Q.-F. Liang, J.-Q. Zheng, X.-J. Zheng, L.-P. Jin, *Dalton Trans*., **2021**, 50, 3916. (c) Y. Chen, Y. Fang, H. Gu, J. Qiang, H. Li, J. Fan, J. Cao, F. Wang, S. Lu, X. Chen, *ACS Appl. Mater. Interfaces*, **2020**, 12, 49, 55094. (d) F. Wu, L. Wang, H. Tang, D. Cao, *Anal. Chem*., **2019**, 91, 8, 5261. (e) M. Mathivanan, B. Tharmalingam, C.-H. Lin, B.V. Pandiyan, V. Thiagaraja, B. Murugesapandian, *CrystEng Comm*, **2020**, 22, 213-228. (f) M. Mathivanan, B. Murugesapandian, *Dyes. Pigm*. **2022**, 203, 110367.

8 (a) Q. Gong, Y. Li, H. Wang, G. Wang, Q. Feng, Y. Zhong, F. Liu, *J. Phys. Chem. C*, **2022**, 126, 43, 18429. (b) J. Jiang, H. Sun, Y. Hu, G. Lu, J. Cui, J. Hao, *Chem. Commun*., **2021**, 57, 7685. (c)

D. Singhal, I. Althagafi, A. Kumar, S. Yadav, A.K. Prasad, R. Pratap, *New J. Chem*., **2020**, 44, 12019. (d) R. Long, C. Tang, Z. Yang, Q. Fu, J. Xu, C. Tong, S. Shi, Y. Guo, D. Wang, *J. Mater. Chem. C*, **2020**, 8, 11860.

9 (a) T. Xiao, C. Bao, L. Zhang, K. Diao, D. Ren, C. Wei, Z.-Y. Li, X.-Q. Sun, *J. Mater. Chem. A*, **2022**, 10, 8528.

10 (a) P. Pallavi, V. Kumar, MD.W. Hussain, A. Patra, *ACS Appl. Mater. Interfaces*, **2018**, 10, 44696-44705. (b) L. Wang, Y. Li, X. You, K. Xu, Q. Feng, J. Wang, Y. Liu, K. Li, H. Hou, *J. Mater. Chem. C*, **2017**, 5, 65.

11 J. Jiang, H. Sun, Y. Hu, G. Lu, J. Cui, J. Hao, *Chem. Commun*., **2021**, 57, 7685-7688.

12 (a) B. Roy, R. Mengji, S. Roy, B. Pal, A. Jana, N.D. Pradeep Singh, *ACS Appl. Mater. Interfaces*, **2022**, 14, 4862−4870. (b) W. Zhang, F. Zhou, Z. Wang, Z. Zhao, A. Qin, B.Z. Tang, *Chem. Asian J.*, **2019**, 14, 1662.

13 X. Shi, N. Yan, G. Niu, S.H.P. Sung, Z. Liu, J. Liu, R.T.K. Kwok, J.W.Y. Lam, W.-X. Wang, H.H.-Y. Sung, I.D. Williams, B.Z. Tang, *Chem. Sci*., **2020**, 11, 3152.

14 (a) K. Bamnavat, V. Bhardwaj, T. Anand, SK Ashok Kumar, S.K. Sahoo, *Dyes Pigm*., **2021**, 184, 108844. (b) K. Wang, B. Feng, G. Wang, J. Cui, L. Yang, K. Jiang, H. Zhang, *Chem. Commun*., **2022**, 58, 2894. (c) S. Barman, S.K. Mukhopadhyay, M. Gangopadhyay, S. Biswas, S. Dey, N.D. Pradeep Singh, *J. Mater. Chem. B*, **2015**, 3, 3490. (d) J. Jayabharathi, V.Kalaiarasi, V. Thanikachalam, K. Jayamoorthy, *J. Fluoresc.*, **2014**, 24, 625.

15 (a) Q. Feng, Y. Li, L. Wang, C. Li, J. Wang, Y. Liu, K. Li, H. Hou, *Chem. Commun*., **2016**, 52, 3123. (b) B. Feng, Y. Zhu, J. Wu, X. Huang, R. Song, L. Huang, X. Feng, W. Zeng, *Chinese Chem. Lett.*, **2021**, 32, 3057. (c) K. Li, Q. Feng, G. Niu, W. Zhang, Y. Li, M. Kang, K. Xu, J. He, H. Hou, B. Z. Tang, ACS Sen., 2018, 3, 920. (d) W. Song, B. Dong, Y. Lu, W. Lin, *Tetrahedron Lett*., **2019**, 60, 26, 1696. (e) L. Daia, W. Maoa, L. Hua, J. Song, Y. Zhang, T. Huang, M. Wang, *Dyes Pigm.*, **2022**, 204, 110436. (f) L. Yan, T. Qing, R. Li, Z. Wang, Z. Qi, *RSC Adv*., **2016**, 6, 63874.

16 (a) Z. Peng, Y. Ji, Z. Huang, B. Tong, J. Shi, Y. Dong, *Mater. Chem. Front*., **2018**, 2, 1175. (b) J. Tong, K. Zhang, J. Wang, H. Li, F. Zhou, Z. Wang, X. Zhang, B. Z. Tang, *J. Mater. Chem.C*, **2020**, 8, 996.

17 (a) Z. Song, R.T.K. Kwok, D. Ding, H. Nie, J.W.Y. Lam, B. Liu, B.Z. Tang, *Chem. Commun*., **2016**, 52, 10076. (b) T. Xiao, C. Bao, L. Zhang, K. Diao, D. Ren, C. Wei, Z.-Y. Li, X.-Q. Sun, *J. Mater. Chem. A*, **2022**, 10, 8528. (c) H. Sun, Y. Jiang, J. Nie, J. Wei, B. Miao, Y. Zhao, L. Zhang, Z. Ni, *Mater. Chem. Front*., **2021**,5, 347.

18 (a) B. Roy, R. Mengji, S. Roy, B. Pal, A. Jana, N.D.P. Singh, *ACS Appl. Mater. Interfaces*, **2022**, 14, 4, 4862. (b) S. Guieu, F. Cardona, J. Rocha, A.M.S. Silva, *Chem. Eur. J.* **2018**, 24, 17262. (c) D. Frath, K. Benelhadj, M. Munch, J. Massue, G. Ulrich, *J. Org. Chem*., **2016**, 81, 9658

19 B. Dutta, S. Halder, *Anal. Methods*, **2022**, 14, 2132.

20 B. Pramanik, D. Das, *J. Phys. Chem. C*, **2018**, 122, 3655.

21 (a) Z. Hu, H. Zhang, Y. Chen, Q. Wang, M.R.J. Elsegood, S.J. Teat, X. Feng, M. Monarul Islam, F. Wua, B.Z. Tang, *Dyes Pigm*., **2020**, 175, 108175. (b) F. Wu, G. Xu, X. Zeng, L. Mu, C. Redshaw, G. Wei, *J. Fluoresc*., **2015**, 25, 5, 1183.

22 A. Kuwar, R. Patil, A. Singh, S.K. Sahoo, J. Marek, N. Singh, *J. Mater. Chem. C*, **2015**, 3, 453.

23 J.J. McKinnon, D. Jayatilaka, M.A. Spackman, *Chem. Commun*., **2007**, 3814.

24 T. Stoerkler, T. Pariat, A.D. Laurent, D. Jacquemin, G. Ulrich, J. Massue, *Eur. J. Org. Chem*., **2022**, e202200661.

25 (a) Y. Liu, B. Feng, X. Cao, G. Tang, H. Liu, F. Chen, M. Liu, Q. Chen, K. Yuan, Y. Gu, X. Feng, W. Zeng, *Analyst*, **2019**, 144, 5136. (b) Z. Song, R.T.K. Kwok, E. Zhao, Z. He, Y. Hong, J.W. Y. Lam, B. Liu, B.Z. Tang, *ACS Appl. Mater. Interfaces*, **2014**, 6, 17245. (c) B. Kumar Dwivedi, V. D. Singh, R. Prasad Paitandi, D.S. Pandey, *ChemPhysChem*., **2018**, 19, 2672.

26 (a) T. Pariat, M. Munch, M. Durko-Maciag, J. Mysliwiec, P. Retailleau, P.M. Vérité, D. Jacquemin, J. Massue, G. Ulrich, *Chem. Eur. J*., **2021**, 27, 10, 3483. (b) M. Munch, E. Colombain, T. Stoerkler, P.M. Vérité, D. Jacquemin, G. Ulrich, J. Massue, *J. Phys. Chem. B*, **2022**, 126, 2108.

27 C. Azarias, S. Budzak, A. D. Laurent, G. Ulrich, D. Jacquemin, *Chem. Sci*., **2016**;120, 2824.

28 G. Narendra Babu, A.R. Balavardhana Rao, Srinivas Keesara, Samudranil Pal, *J. Organomet. Chem*., **2017**, 243.

29 T. Pariat, T. Stoerkler, C. Diguet, A.D. Laurent, D. Jacquemin, G. Ulrich, J. Massue, *J. Org. Chem*., **2021**, 186, 17606.

30 A ^{13}C NMR spectrum was not obtained due to inherent low solubility in $CDCl_3$ or DMSO.

Table of contents (TOC)

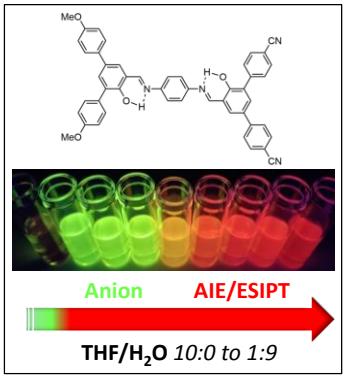

This article describes a series of heteroaryl-substituted bis-anil derivatives presenting aggregation-induced emission (AIE) coupled with an excited-state intramolecular proton transfer (ESIPT) process.